Journal of Materials Chemistry B

Accepted Manuscript

ROYAL SOCIETY OF CHEMISTRY

www.rsc.org/materialsB

Journal of
Materials Chemistry B

RSCPublishing

ARTICLE

Kaolin-reinforced 3D MBG scaffolds with hierarchical architecture and robust mechanical strength for bone tissue engineering†

Cite this: DOI: 10.1039/x0xx00000x

Received
Accepted

DOI: 10.1039/x0xx00000x

www.rsc.org/

Wei Tang,[abc] Yuan Yuan,[*ab] Dan Lin,[bc] Haoyi Niu,[bc] and Changsheng Liu[*abc]

Three-dimensional mesoporous bioglass scaffolds (3D MBG) with mesoporous structure and highly interconnected macroporous networks are considered as ideal biomaterials for skeletal tissue applications. However, the inherent brittleness and poor mechanical strength greatly hamper their performance and clinical application. Here, by a modified polyurethane foam (PU) templating method with utilization of kaolin as binder, a new facile method for preparation of 3D MBG scaffold with excellent mechanical strength, mineralization ability and desirable cellular response was proposed. The developed hybrid MBG-XK (where X refers to the final dry weight of Kaolin in the scaffold) scaffolds with 85% porosity exhibited a high compressive strength from 2.6 to 6.0 MPa with the increasing content of Kaolin (5%-20%), about 100 times higher than the traditional PU-template MBG scaffold. With the addition of Kaolin, the MBG-10K scaffold exhibited a more stable and desirable pH environment, and enhanced protein adsorption capacity. Furthermore, with rat bone marrow stromal cells (rBMSCs) as a model, in vitro cell culture experiments indicated that compared with MBG, the prepared MBG-XK scaffold possessed comparable cell proliferation, penetration capacity, enhanced cell attachment and osteogenic differentiation, especially for MBG-10K.

Introduction

Segmental/critical-sized bone defects, delayed bone unions and pseudarthrosis in orthopaedic and maxillofacial surgery represent common and significant clinical problems that have tremendously driven the research of bone tissue regeneration.[1, 2] An ideal scaffold proposed for bone regeneration should be biodegradable and biocompatible, with highly interconnected hierarchical pore structure and robust mechanical strength.[3-5] Since its inception, mesoporous bioactive glasses (MBG) have been considered as excellent candidate for fabrication of bone scaffold with hierarchical architecture.[6, 7] Forerunners, Zhao et al found the superior bone-forming bioactivities of MBG and opened up a promising application of MBG in the field of bone tissue engineering in 2004.[8] However, MBG's inherent brittleness and generally low mechanical strength greatly undermine its biologic performances, thereby, hamper its clinical application.[9] In light of these limitations, it is imperative to develop a 3D MBG scaffold with excellent mechanical property and architecture similar to that of cancellous bone.

Traditionally, methods used for preparation of MBG scaffolds mainly include the polyurethane sponge (PU) templating method,[10] 3D printing technique,[11] and porogen-based process. Only the two former methods can generate highly interconnected macropores. Although the MBG scaffolds prepared by PU methods possess optimized interconnected pores, they are quite brittle and unable to overcome the typical handicap of poor mechanical strength (55 kPa).[12, 13] Recently, by PU template method, Wang et al.[12] and Xiao et al.[13] have developed Zr-incorporated MBG scaffold and silk-modified MBG scaffold with enhanced mechanical strength. But, the compressive strength is only 214 kPa and 250 kPa, respectively, which is still fragile and much lower than the compressive strength of human trabecular bone (2-12 MPa).[14] To solve this drawback, many researchers have proposed the 3D printing technique.[10, 15] which can improve the mechanical strength of 3D MBG scaffold. Unfortunately, the mixture of polymer (such as PVA, PCL etc.) with/in MBG may compromise the unique mesoporous structure or biological properties of MBG to some extent.[3, 16] Meanwhile, the process often requires a special printing instrument. Therefore, it is essential to develop an alternative, simple strategy to fabricate high-performance 3D MBG scaffold at low cost.

Kaolin, a native hydrated aluminium silicate that consists of microporous particles, has been well established as a reinforcing agent,[17, 18] adsorptive biomaterial,[19] and blood

clotting agent,[20-22] in commercial biomedical materials, and shows excellent mechanical strength, nontoxic and non-immunogenic properties.[23] Also, kaolin has been applied for human bone replacement.[23] These advantages of Kaolin motivated us to hypothesize that incorporation of Kaolin may improve the mechanical properties of MBG scaffolds while maintaining or possibly enhancing its osteoactivity.

For this purpose, a facile and reproducible strategy was reported here to create a robust MBG-XK scaffold by a "one-step-casting" PU templating process. To ensure the formation of homogeneous and interconnected pores, the sol viscosity and kaolin content were concisely controlled. The effects of the Kaolin content on the mesostructure, mechanical strength and apatite-forming capacity of the resulting scaffolds were investigated. Moreover, with rBMSCs as an in vitro model, we further evaluated cell proliferation, attachment and osteogenic differentiation on the modified scaffolds.

Experimental

Material

P123 (M_W=5800, $EO_{20}PO_{70}EO_{20}$), 3-(4,5-dimethylthiazol-2-yl)-2,5-diphenyltetrazolium bromide (MTT), dimethyl sulfoxide (DMSO), fluorescein isothiocyanate-Phalloidin (FITC-Phalloidin), 2-(4-Amidinophenyl)-6-indolecarbamidine dihydrochloride (DAPI) and Alizarin Red were all from Sigma-Aldrich (CA, USA). Tetraethyl orthosilicate (TEOS) and triethyl phosphate (TEP) were from Shanghai Lingfeng Chemical Reagent Co. Ltd. (Shanghai, China). Ethanol, $Ca(NO_3)_2{\cdot}4H_2O$, hydroxymethyl aminomethane-HCl (Tris-HCl) and $Al_2O_3{\cdot}2SiO_2{\cdot}2H_2O$ (Kaolin) were from Sinopharm Chemical Reagent Co. Ltd. (Shanghai, China). BCA protein assay kit was purchased from Beyotime Biotech Co. Ltd (Jiangsu, China). All reagents used in cell culture were from Gibco (Grand Island, NY).

Synthesis of MBG-based scaffolds with different amounts of Kaolin

Kaolin-reinforced 3D MBG scaffold was synthesized by sol-gel and modified polyurethane sponge templating method. The modified scaffolds with 5%, 10% and 20% of kaolin (mass ratio) will be referred to as MBG-5K, MBG-10K and MBG-20K, respectively. Here, MBG-10K is used as an example to describe the detailed synthesis process.

In a typical reaction, 4.0 g P123, 6.7 g TEOS, 1.4 g $Ca(NO_3)_2{\cdot}4H_2O$, 0.73 g TEP and 1.0 mL HCl (0.5 M) were dissolved in 60 mL of ethanol and stirred at 40 °C for 1 d.[8] Next, the sample was evaporated under vacuum condition for 30 min at 60 °C. Thereby, a MBG sol with a viscosity of 5×10^4 Pa.s was obtained. Afterwards, the viscous sol was homogeneously mixed with Kaolin particles. Kaolin was maintained at 10% of the final dry weights of the composite MBG scaffold. Then, polyurethane (PU) sponge with desired shape was completely squeezed in the hybrid MBG-10K slurry until the slurry was uniformly coated on the struts of PU sponge (0.5 g/cm^3, with a corresponding porosity is 85%). The products were dried at 60 °C for 72 h and calcinated at 600 °C (1 °C/min) for 5 h to obtain the final MBG-10K scaffolds. All chemical compositions and contents of Kaolin in scaffolds are listed in Table 1.

Table 1 Chemical composition and amounts of Kaolin (dry-weight) in calcined scaffolds

Sample Name	Molar ratio Si: Ca: P	MBG (g)	Kaolin (g)
MBG	80:15:5	6	0
MBG-5K	80:15:5	6	0.32
MBG-10K	80:15:5	6	0.67
MBG-20K	80:15:5	6	1.5

Characterization of MBG-XK scaffolds

The ordered mesoporous structure of MBG-XK was confirmed by X-ray diffraction (XRD, Rigaku, Japan) and transmission electron microscopy (TEM, JEM-2100, Japan). Surface analysis of mesoporous structures was performed by nitrogen isothermal adsorption with a Micromeritics ASAP2010 sorptometer (Micromeritics, USA). Surface area was calculated using Brunauer-Emmett-Teller (BET) method, and pore size distribution was calculated by Barrett-Joyner-Halenda (BJH) method. Microstructure and surface morphology of the scaffolds was observed under a scanning electron microscope (SEM, JSM-6360LV, JEOL, Japan). The composition and Kaolin distribution were analysed by energy dispersive spectrometry (EDS, Falcon, USA)

Porosity of the prepared scaffold was measured using Archimedes' principle: porosity (%)= $(W_2–W_1)/(W_2–W_3) \times 100\%$, where W_1 is dry weight of the scaffold, W_2 is weight of the scaffold saturated with water, and W_3 is the weight of the scaffolds suspended in water. Five samples were tested to calculate the average porosity.

Mechanical strength of MBG-XK scaffolds

The mechanical strength of MBG-XK scaffold ($10 \times 10 \times 10$ mm^3) was measured using a universal testing machine (AG-2000A, Shimadzu, Japan) at a constant loading rate of 1 mm/min. With the viscosity remain constant, the porosity can be adjusted by the mass to volume ratio of the hybrid sol. For each composition, four specimens were tested, and the results were averaged.

In vitro bioactivity and biodegradation

The in-vitro bioactivity was studied by monitoring the formation of hydroxyapatite (HA) on the sample surface with time 0.1 g of scaffold was soaked in 25 mL SBF at 37 °C for 3 and 7 d. Apatite mineralization was evaluated by SEM for morphological observation, EDS and Fourier transform infrared spectroscopy (FTIR, Nicolet 380, Thermo Electrics, USA) for compositional analysis. Moreover, weight loss of the MBG-XK scaffolds was calculated from the ionic dissolution of SiO_4^{4-} ions at different time by inductively coupled plasma-atomic emission spectroscopy. (ICP-AES, IRIS 1000, Thermo Elemental, USA). Weight loss of the scaffolds (W) was calculated by the equation: $W = (c_{Si} \times v_{Si}) / m_{Si} \times 100\%$, where c_{Si}, v_{Si} and m_{Si} represent the Si concentration in SBF, volume of SBF (mL) and Si content (mg) of the scaffolds soaked in SBF.

In addition, pH value, ionic dissolution and protein adsorption capability of the scaffolds were tested after soaking the scaffolds in α-MEM containing 10% FBS for 24 h (0.01 g scaffold / 1 mL α-MEM).

Isolation and culture of rBMSCs

The rBMSCs were extracted from rat bone marrow. Both ends of the rat femur were cut away from the epiphysis. Bone marrow was

flushed out with 15 mL culture medium (α-MEM) containing 10% foetal bovine serum (FBS) and 1% antibiotics (100 U/mL penicillin G and 100 U/mL streptomycin sulphate). The bone marrow suspension was poured into a 75 cm^2 tissue culture polystyrene flask and incubated at 37 °C in a humidified atmosphere containing 5% CO_2. The culture medium was refreshed every 2 d until about 90% confluence was achieved.

Cell culture on MBG-XK scaffolds

First, MBG-XK scaffolds (10 × 10 × 3 mm^3) were placed at the bottom of each well of a 24-well cell culture plate and pre-soaked in culture medium for 24 h. Next, 100 μL rBMSCs suspension was seeded on each sample and incubated in a humidified atmosphere of 5% CO_2 at 37 °C for 2 h to allow for rBMSCs attachment. After that, 900 μL of culture medium was added to each well. The rBMSCs attached to the scaffolds were cultured in a humidified atmosphere of 5% CO_2 at 37 °C for other experiments.

Cell attachment and morphology

For studies of cell attachment, a seeding density of 1.0 × 10^5 cells/sample was applied. After 6 h incubation, samples were washed with phosphate-buffered saline (PBS) twice and fixed with formalin solution (3.7% formaldehyde in PBS) for 15 min. The fixed cells were washed with PBS for three times and dehydrated in ascending concentrations of ethanol (30%, 50%, 70%, 90%, 95% and 100%, v/v%) for 5 min at each gradient. Samples were then immersed in isoamyl acetate for 20 min and vacuum-dried at 37 °C for 4 h. Cell attachment on the dried specimens was observed using SEM (S-3400, Hitachi, Japan). The initial cell adhesion on the scaffolds after culturing for 2 or 6 h was also tested by MTT.

Moreover, cell morphology and spreading were visualized using confocal laser-scanning microscopy (CLSM, Nikon, Japan). After 24 h of incubation, cytoskeleton was stained with FITC-Phalloidin (5 μg/mL) for 40 min and cellular nuclei were counterstained with DAPI (5 μg/mL) for 10 min. Then all specimens were observed using CLSM.

Cell viability and proliferation

Cell proliferation was evaluated by MTT assay. In brief, rBMSCs were cultured on equal amounts of MBG-XK scaffolds in 24-well culture plates at a density of 2.0 × 10^4 cells/well. After 1, 3 and 7 days of culture, 30μL MTT solution (5 mg/mL) was added. Cells were then incubated at 37 °C for 4 h to allow the formation of formazan crystals, which were subsequently dissolved using DMSO. The optical density (OD) was measured at 492 nm using a microplate reader (SPECTRAmax 384, Molecular Devices, USA).

Cell osteogenic differentiation assay

Alkaline phosphatase (ALP), an indicator of early differentiation of osteoblast-like cells, was measured after the cells were cultured with the scaffolds for 7 d. To evaluate ALP activity, rBMSCs were seeded on MBG and MBG-XK scaffolds at a density of 2 × 10^4 cells/well. After 7 days of culture, the maintenance medium was removed, and 200 μL Nonidet P-40 (NP-40, 1%) solution was added to each well at room temperature. Samples were incubated for 1 h to obtain cell lysates. Then, 50 μL of the cell lysates from each sample was added to 96-well plates. 50 μL of 2 mg/mL *p*-nitrophenyl phosphate substrate solution (pNPP, Sangon, Shanghai, China), containing 0.1 mol/L glycine and 1 mmol/L $MgCl{\cdot}6H_2O$ was added and incubated for 2 h at 37 °C, the reaction was quenched by adding 100 μL NaOH (0.1 mol/L) and the absorbance of ALP was quantified at a wavelength of 405 nm using a microplate reader. The total protein content in each cell lysate was determined using a BCA assay kit. ALP levels were normalized to the total protein content, and all experiments were performed in quadruplicate.

Mineralization of rBMSCs was analysed on day 14 by Alizarin Red staining. At the end of the incubation period, cells were washed with PBS at room temperature and fixed with formalin solution. Fixed cells were stained with 1% Alizarin Red (pH = 4.2) for 10 min. The cells were then rinsed with water and viewed with an inverted light microscope (TE2000U, Nikon Corp., Japan).

Statistics Analysis

Results were expressed as means ± standard deviations. All data were generated using more than three independent experiments. Statistical analysis was conducted using one-way analysis of variance (ANOVA). A value of $p < 0.05$ was considered as statistical significance.

Results and discussion

Preparation and characterization of MBG-XK scaffolds

Sol-gel and PU foam template processes have been successfully utilized to prepare MBG-based scaffolds. In a traditional process, the precursor sol with low viscosity is directly cast into PU sponge, and the excess sol is removed by squeezing. To increase the amount of MBG attached onto the PU strut, the "casting-squeezing-drying" process often repeats several times and thus results in a heterogeneous and non-continuous macroporous structure.[24] This flawed structure may be detrimental to the mechanical strength and further affect the ensuing performance of MBG to some extent.

To address this problem, in our modified process as illustrated in Scheme 1, the sol viscosity were tightly controlled at about 5×10^4 Pa.s and Kaolin was adopted as reinforcing agent. Importantly, the viscosity of MBG sol was essential to yield a faithfully replicated PU macrostructure without heterogeneous frameworks or formation of a cage-like structure.[25] After mixed with Kaolin, the composite MBG-XK slurry was uniformly impregnated onto the PU struts. With the removal of the templates by calcination, the MBG-XK scaffolds with interconnected macrostructure and excellent mechanical property were successfully prepared. (see Fig. S1)

The characters of Kaolin particle were investigated and presented in Fig. 1. Drawn from the TEM images (Fig. 1A), Kaolin showed good dispensability and the average particle size was under 1μm.

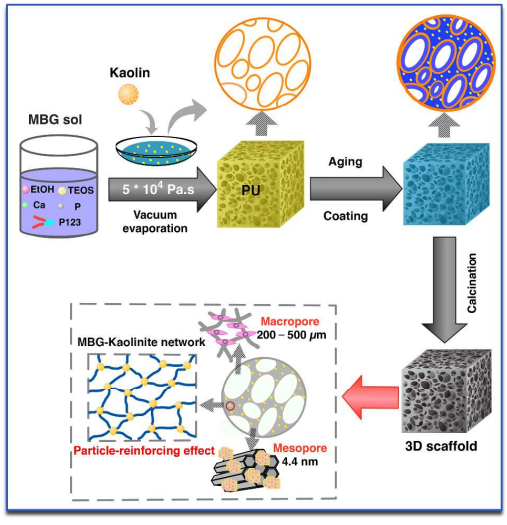

Scheme 1 Schematic illustration of the modified process for preparation of MBG-XK scaffolds with excellent mechanical properties and superior cellular behavior.

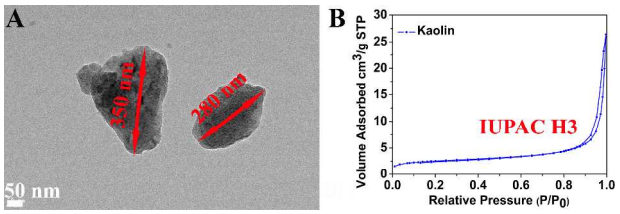

Fig. 1 Characterization of Kaolin particles. (A) TEM image of the Kaolin particles. (B) N_2 adsorption-desorption isotherm of Kaolin particles with type H3 isotherm, which is s typical slit-shaped microstructure.

According to the N_2 adsorption-desorption analysis (Fig. 1B), the hysteresis curve shape was close to a IUPAC H3 standard, which corresponds to slit-shaped pores.

To gain insight into the hierarchically porous property, Fig. 2 shows the macroporous morphology and mesoporous structure of the prepared scaffolds. From the representative SEM images (Fig. 2A1-D1), it can be seen that all scaffolds exhibited an interconnected macroporous structure with average pore diameter about 200-500 μm and a wall thickness of 50-80 μm. As anticipated, a quite uniform pore morphology was observed at high magnifications. This confirmed our hypothesis that this modified method could improve the homogeneity and continuity of scaffold. Fig. 2 A2-D2 revealed that the addition of kaolin particles decreased the smoothness of macropore wall, in particular for the MBG-10K and -20K, but there is no large agglomerate on the pore surface.

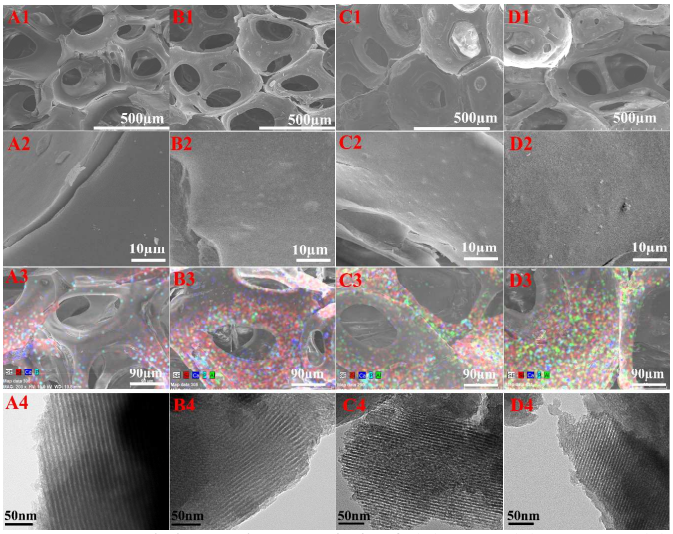

Fig. 2 SEM Morphology and EDS analysis of (A) MBG, (B) MBG-5K, (C) MBG-10K and (D) MBG-20K scaffolds with different Kaolin content. (A1-D1) SEM images of the macroporous structure and (A2-D2) topographic surfaces. (A3-D3) EDS surface scanning of the scaffolds that different colour represent the distribution of elements (red, blue, cyan and green refer to the Si, Ca, P, Al, respectively). (A4-D4) TEM images of the mesostructure in the macropore walls. The developed MBG-XK scaffolds here presented a quite uniform interconnected macroporous network (200-500 μm) and well-ordered mesopore channel (4.4 nm).

The element distribution in EDS scanning (Fig. 2A3-D3) confirmed the uniform distribution of Kaolin in the MBG matrix. Moreover, drawn from the TEM image (Fig. 2A4-D4), the MBG-XK scaffolds exhibited typical hexagonally arranged patterns as MBG, indicating a homogeneous mesopore structure assembled in the confined macro-strut. Corresponding results were further demonstrated in SAXRD pattern (Fig. 3A) with a typical diffraction peak around 2θ=1.2°. Due to the non-mesostructure nature of Kaolin, the diffraction peaks of MBG-XK scaffolds broadened slightly and the diffraction intensities decreased to a certain extent. Correspondingly, the diffraction peaks of WAXRD pattern (Fig. 3B) in MBG-XK were significantly increased at 2θ=26.6, which associated with the de-hydroxylation process of kaolin at 600 °C. Moreover, the FTIR spectra of the MBG-XK samples (Fig. S2) with relative decreased intensity at 793 cm-1 and increased peak at 695 cm-1 further confirmed the successful incorporation of Kaolin into MBG matrix.

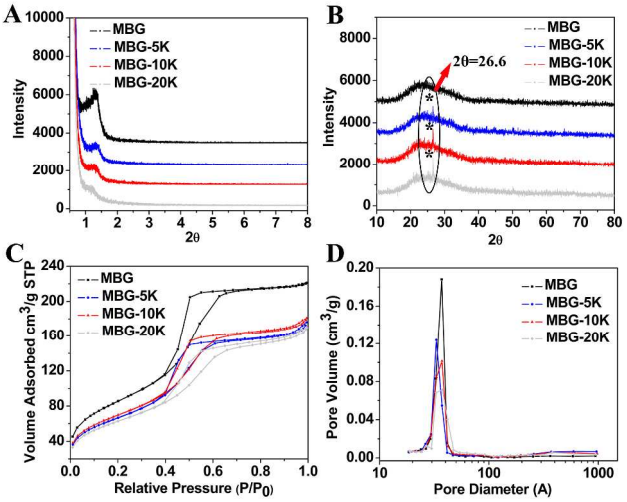

Fig. 3 (A) WAXRD and (B) SAXRD patterns of the MBG and MBG-XK scaffolds. (C) N_2 adsorption-desorption isotherms and (D) the corresponding pore size distributions of the scaffolds. A typically IV isotherm pattern was observed in N_2 adsorption-desorption analysis of the MBG-XK scaffold and the corresponding mesopore size distribution is about 4.4 nm.

Similar to the ordered mesoporous structure in MBG reported previously,[8] an obvious capillary condensation step at a relative pressure of P/P_0=0.4-0.6 was observed in N_2 adsorption-desorption analysis (Fig. 3C). According to the BJH model, it suggested a uniform but small pore size distribution of 4.4 nm (Fig. 3D). The total pore volumes and BET surface areas for MBG-XK samples are summarized in Table 2**.** The pure MBG scaffolds had the highest surface area (312.7 m^2/g) and the surface areas decreased with Kaolin addition (263.8, 254.6 and 229.8 m^2/g for MBG-5K, -10K and -20K, respectively).

These results indicated that the addition of Kaolin in 5-20% had no obvious effect on the mesoporous structure and exhibited a significantly enhanced moulding capability and structural stability. The overall macro-scaled structure and the inner nano-scaled environment will provide ideal biochemical environments for cell anchorage and drug delivery, implying an excellent candidate as graft for bone tissue regeneration.

Table 2 Mesoporous properties of the MBG and MBG-XK scaffolds.

Sample Name	BET surface area (m^2/g)	Pore volume (cm^3/g)	Average pore size(nm)
MBG	312.7	0.338	4.33
MBG-5K	263.8	0.283	4.47
MBG-10K	254.6	0.280	4.40
MBG-20K	229.8	0.263	4.57

Mechanical strength of the MBG-XK scaffolds

For the regeneration of hard tissues, 3D scaffold should provide adequate mechanical property to match the growth of tissues at the site of implantation. Fig. 4 shows the load/displacement graph of the MBG-XK scaffolds under compressive testing. A high porosity of the scaffold often leads to low compression strength. With the kaolin content increased from 0% to 20%, the compressive strength of the scaffolds was considerably increased from 0.3 to 6 MPa at a high porosity of 85%. The dependence of the mechanical strength of MBG-XK scaffolds on porosity and Kaolin content are listed in Table 3.

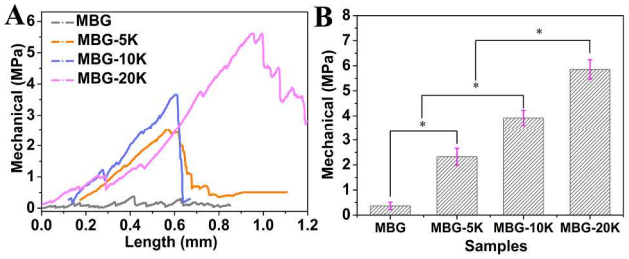

Fig. 4 (A) The compressive strength of the MBG and MBG-XK scaffolds. MBG/Kaolin scaffolds have greater strength than MBG scaffolds. (B) The average mechanical strength of porous scaffolds. The Kaolin incorporation in the MBGs scaffolds demonstrated an enhanced mechanical strength with highly porosity of 85%. Asterisk indicates significant differences, $p < 0.05$.

Table 3 Summary of the mechanical properties of the prepared scaffolds

Sample Name	Mechanical strength (MPa)		
	Porosity: 65%	Porosity: 75%	Porosity: 85%
MBG	0.6±0.1	0.45±0.1	0.3±0.1
MBG-5K	4.8±0.2	3.6±0.2	2.5±0.2
MBG-10K	7.2±0.2	5.6±0.2	4.0±0.2
MBG-20K	9.5±0.2	7.8±0.2	6.0±0.2

Based on the previous reports and the results here, two possible reasons can be attributable to the significantly improved mechanical strength of MBG-XK. One is the controlled viscosity of MBG sol used for impregnation. In the experiment, we found that a suitable viscosity played an important role for penetration and distribution of the MBG-XK sol and in turn exerted great effects on the macrostructure and mechanical strength of the final scaffolds. If the viscosity is too low, as observed in traditional sol-gel-PU template processes, the repeated casting-squeezing-drying process results in a non-continuous macronetwork. What's worse, the MBG sol forms "cell membranes" on the adjacent struts, which is more like a "cage" structure without interconnected property. On the other hand, too high viscosity results in a poor penetration property, yielding a scaffold with a "thick outer and thin inner strut" heterogeneous distribution, even after squeezing. Herein, the viscosity of the MBG sol was modulated at 5×10^4 Pa.s to make sure the slurry with desirable rheological characteristics and thus obtained a faithfully replicated PU macrostructure with a uniform and stable structure.

The other is possibly related to the typical "particle-reinforcing" effect of Kaolin (Scheme 1). In the composite system, kaolin was well dispersed in MBG matrix and formed a good bridging between the MBG matrix.[26, 27] Due to the high capillary pressure pores in Kaolin particles, MBG sol could contact with the particles completely and formed a crosslinking network among them. During calcination, the dispersed Kaolin particles underwent an important de-hydroxylation process and thus formed a reactive interface,[28] which could give rise to intense secondary interaction between MBG and Kaolin. Consequently, with homogenous Kaolin distribution and interpenetration between Kaolin and MBG matrix, the Kaolin/MBG network was formed, which could efficiently absorb and dilute impact energy.

Compared with previous study, our method is more operable and produces more homogeneous and continuous macrostructure. Most importantly, the MBG-XK scaffolds obtained here possess considerably improved mechanical strength, comparable or even superior to that of 3D printing method.[29]

In vitro mineralization, weight loss, pH change and adsorption property of MBG-XK scaffolds

As far as changes in chemical composition and specific surface structure, the bioactivity of MBG-XK scaffold was examined. With MBG-10K as example, after biologic solution soaking for 3 and 7 d, the surface of MBG-10K scaffold underwent important changes that a layer of apatite formed on the macropore wall with flake-like shapes (Fig. 5A-C). The specific EDS analysis indicated a corresponding rising Ca/P ratio over time. Moreover, additional P-O peak at around 566 and 967.5 cm^{-1} corresponded to bending vibration in the PO_4^{-3} tetrahedron, and vibrational peaks at 1425.6 and 875 cm^{-1} assigned to the C-O vibration bands appeared at 3 d in the FTIR pattern (Fig. 5D), which further confirmed the newly formed apatite on the surface.[30] Other MBG-XK samples exhibited similar phenomenon.

Next, Fig. 5E shows dissolution profiles for MBG-10K scaffolds over time, which is calculated from the Si ion released in SBF (Fig. S3). It is known that ion release is an important factor contributing to the degradation of materials. ICP analysis demonstrated a more gentle dissolution rate in kaolin-containing scaffolds during the entire experimental period. After soaking in biological solution for 7 d, the weight loss of MBG-10K was about 3.88%.

Recently, it has been widely reported that fast dissolution of MBG can result in a high pH value in the surrounding environment, which

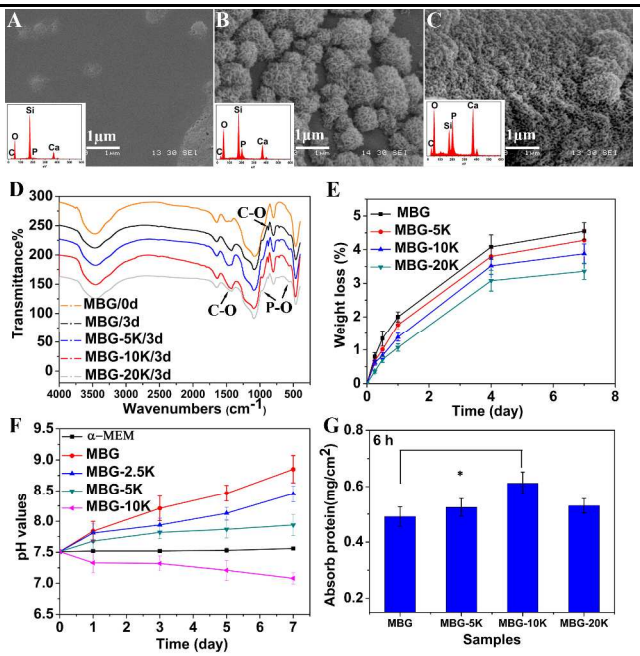

Fig. 5 (A-C) SEM images and EDS patterns (insert) of the MBG-10K scaffold before and after soaking in SBF for 3 and 7 days, respectively (porosity: 85%). (D) FTIR spectra of MBG-XK scaffolds after soaking in SBF for 3 days. (E) Degradation profiles of MBG-XK scaffolds after soaking in SBF for different times. (F) pH values of α-MEM after MBG-XK soaking. (G) Protein absorbed on MBG-XK scaffolds after soaking in α-MEM containing 10% FBS for 6 h. MBG-10K exhibited inspiring properties in terms of mineralization, degradation rate, pH stabilization and protein adsorption. Asterisk indicates significant differences, $p < 0.05$.

will adversely affect cell response.[31] Here, the pH changes of α-MEM culture medium MBG-XK soaking are shown in Fig. 5F. It's worth noted that MBG-XK scaffolds had a stabilized pH environment. When the duration was increased from 1 to 7 days, the pH value of pure MBG in α-MEM solution increased over 9. But, in the case of MBG-XK scaffolds, especially for MBG-10K, the pH was maintained around 8. This result indicated that the Kaolin played an important role in pH stabilization at normal physiological level (7.4), which could prevent cell damage due to pH variation.

Moreover, in order to elucidate the protein adsorption on MBG-XK scaffolds, all scaffolds were soaked in α-MEM containing 10% FBS (Fig. 5G). Interestingly, 0.61 mg/cm^2 protein absorption was observed on MBG-10K scaffold, about 25% increased in comparison with MBG. Compared to the MGB, there are two contradictory aspects that might influence their protein adsorption capacity of the MBG-XK. One is the remarkable adsorptive capacity and reactive de-hydroxylation of Kaolin, the other is the decreased mesoporous surface area due to the incorporation of Kaolin. We speculate, in MBG-10K, the former aspect might slightly dominate, while in MBG-5K and MBG-20K, two aspects balanced themselves out.

Cell attachment and proliferation

Cell attachment is the first step of cell/biomaterial interaction which directly affects the ensuing biological properties.[32] The initial cell attachment on MBG-XK scaffolds was evaluated after 6 h cultivation. As shown in Fig. 6A-D, rBMSCs spreaded well on the surface of the pore walls with pseudopodia. And there were significant differences in the cell morphology on different samples. Particularly, a larger number of prominent filopodia and unidirectional lamellipodia extensions of rBMSCs were observed on the MBG-10K and MBG-20K scaffolds. In addition, cell spreading area, perimeter, and Feret's diameter calculated from Image J quantitatively confirmed the results (Fig. 6E-G). The number of the initial cell attachment at 2 and 6 h measured by MTT assay (Fig. 6H) also indicated an enhanced cell attachment on the MBG-10K scaffold. Previous studies have reported that surface topography,[33] porosity,[34] wettability,[35] surface stability,[36] pH value[31] often play critical role in modulating protein adsorption and ensuing cell attachment. So, we believe that the rough surface, interconnected macrostructure and native hydrophilicity of MBG and Kaolin and thus the excellent protein adsorption capacity, together with the desirable pH environment, may contribute to the enhancement of cell attachment on MBG-10K.

Furthermore, cell penetration and ingrowth analysis after seeding on the MBG-10K surface for 24 h were shown in Fig. 7A-D. The 3D visualization of the images revealed that the cells penetrated deeply into the scaffold (deeper than 200 μm) and anchored with intimate contact along the macropore walls with an elongated and spindle-shaped morphology. Moreover, drawn from the MTT results in Fig. S4, the Kaolin had no obvious toxicity on cell proliferation of MBG-XK scaffolds.

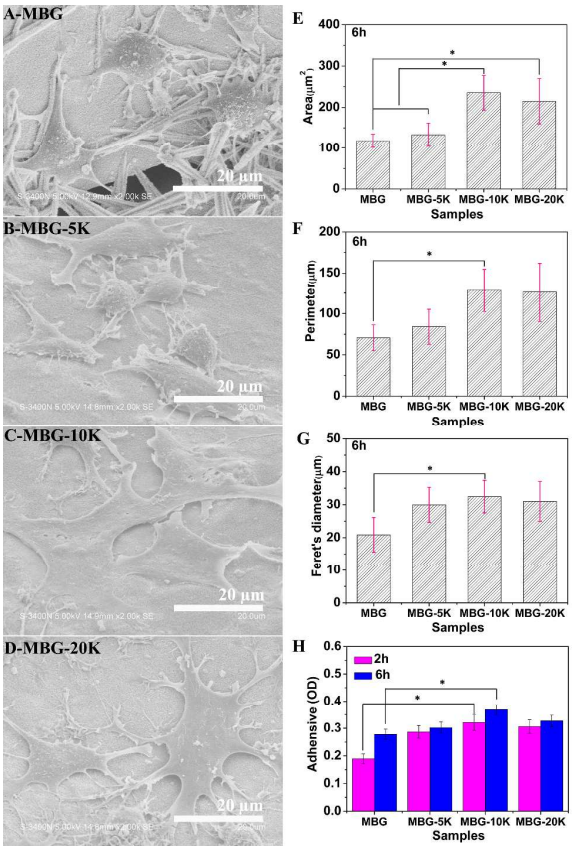

Fig. 6 Cell morphology and attachment of rBMSCs on MBG-XK scaffolds with different Kaolin contents. (A-D) SEM images of cell morphology on MBG and MBG-XK scaffolds for 6 h. (E-G) Image J analysis of cell area, perimeter and Feret's diameter on scaffolds. (H) The initial cell adhesion on the samples after culturing for 2 and 6 h by MTT test. Significantly, Kaolin incorporated into MBG scaffolds enhanced cell attachment in vitro, particularly for the MBG-10K. Asterisk indicates significant differences, $p < 0.05$.

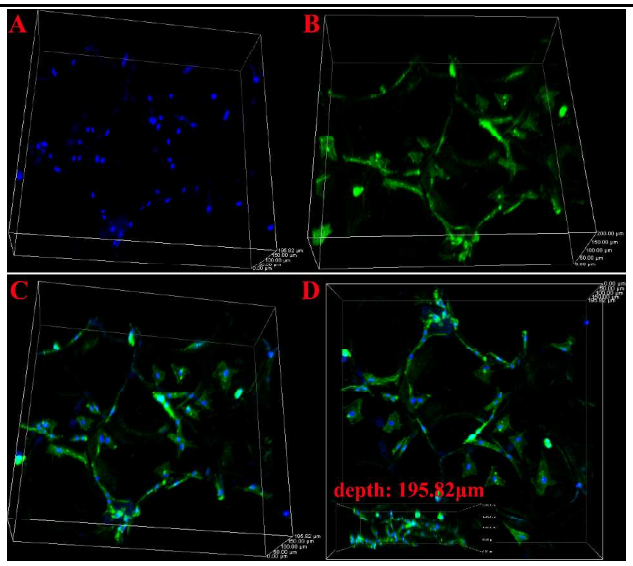

Fig. 7 Cell adhesion and ingrowth analysis of rBMSCs on the surface of MBG-10K scaffold at 24 h. Confocal laser scanning microscopy: (A-D) 3D visualization of rBMSCs on MBG-10K scaffold. Cytoskeleton stained with FITC-Phalloidin (green) and cellular nuclei counterstained with DAPI (blue).

Cell osteogenic differentiation assay

A suitable artificial should not only provide a structural support for bone cells, but also induce bone formation by stimulating osteoblastic cell proliferation and differentiation.[5, 31, 32] In order to evaluate the differentiation of rBMSCs cultured on different Kaolin content scaffolds, ALP activity (Fig. 8A) and mineralization (Fig. 8C-E) were measured in this work. The MBG-10K scaffold exhibited higher ALP activity and mineralization to the other scaffolds.

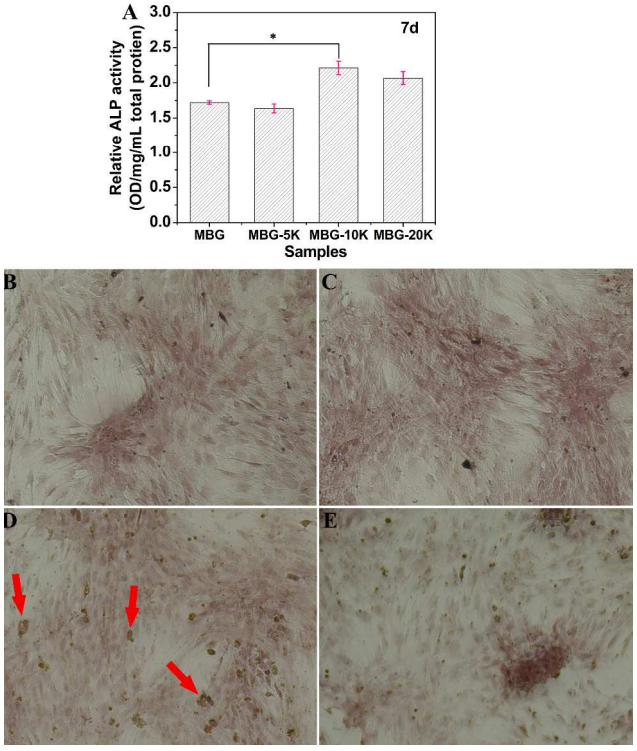

Fig. 8 Osteogenic differentiation of rBMSCs on various scaffolds. (A) The ALP activity after 7 d of culture. Alizarin Red staining of rBMSCs on (B) MBG, (C) MBG-5K, (D) MBG-10K and (E) MBG-20K scaffolds for 14 d (magnification of 100). Obviously, the MBG-10K scaffold exhibited overwhelmingly superior ALP activity and mineralization than other scaffolds. Asterisk indicates significant differences, $p < 0.05$.

Based on previous investigations, three factors were abstracted to explain the mechanism of the enhanced osteogenic differentiation as follows. The first is the ions dissolution from the scaffold as it is well accepted that bioactive silicate glasses are able to stimulate ostegenesis.[31] Specifically, Hench[37] reported that Ca and Si respective concentration of 60-88 ppm and 17-21 ppm is critical for up-regulating several osteogenic genes. Similar results have also been observed by Wu et al,[38] that Si ions at 0.625 mM could significantly enhance mineralization, bone-related gene expression, Wnt and Shh signalling pathway of rBMSCs. In addition, as the main components of the inorganic phase of human bone, Ca and P also play an important role in bone formation and resorption.[39] As observed by Maeno et al,[40] only low (2-4 mmol) Ca concentrations are suitable for osteoblast proliferation and differentiation, whereas higher Ca concentrations (>10 mmol) are cytotoxic. After soaked in α-MEM for 24 h, the concentration of Si, Ca and P dissolved from the MBG-10K scaffold reached 20 ppm, 85 ppm and 4.8 ppm (Fig. S5), respectively, consistent with the above reported ions concentration favorable for osteogenic differentiation. The cell osteogenic differentiation cultured with scaffold extracts exhibited the similar trend (**Fig. S6**) The second factor is the appropriate environment for cell growth. Previous studies have indicated that the high pH value in the surrounding environment would undermine cell growth and osteogenic ability.[12] Therefore, the optimal pH environment of MBG-XK scaffolds may be another important factor benefiting the differentiation of rBMSCs. The third aspect is the surface properties of MBG-10K. It would greatly influence the interactions between cells and implants through eliciting controlled cellular adhesion and maintaining differentiated phenotypic expression.[41] In addition, it has been reported that flat cell morphology with fully spreading shape and regular cytoskeleton is favourable for cell differentiation.[42] Thus, the elongated and highly branched osteogenic morphology of rBMSCs on MBG-10K surface was also good for the enhanced mineralization outcome. Yet, further research might be needed to gain a deeper understanding of the underling mechanism.

Conclusion

Based on the above rationale, the combination of Kaolin brings about a significant enhancement of moulding capabilities and mechanical properties of MBG scaffold. The improved mechanical strength is up to 6.0 MPa even at a high porosity of 85%. The novel MBG-XK scaffold presented uniform interconnected macropores network (200-500 μm) and mesostructure (4.4 nm), as well as good bioactivity and proper degradation rate. With the superior biocompatibility of MBG-10K scaffolds in terms of cell attachment and osteogenic differentiation, the hybrid scaffolds will provide an excellent candidate for bone tissue regeneration.

Acknowledgements

The authors wish to express their gratitude for financial support from the National Basic Research Program of China (973 Program, No. 2012CB933600), National Natural Science Foundation of China (No. 31100679) and Shanghai Nanotechnology Special Foundation (No. 11nm0506300). This study was also supported by the Program for New Century Excellent Talents in University (No. NCET-11-0640).

Notes and references

[a] The State Key Laboratory of Bioreactor Engineering, East China University of Science and Technology, Shanghai 200237, PR China.
[b] Key Laboratory for Ultrafine Materials of Ministry of Education, East China University of Science and Technology, Shanghai 200237, PR China.
[c] Engineering Research Centre for Biomedical Materials of Ministry of Education, East China University of Science and Technology, Shanghai 200237, PR China.

1. S. Bose, M. Roy and A. Bandyopadhyay, *Trends in biotechnology*, 2012, 30, 546-554.
2. D. Zou, Z. Zhang, J. He, S. Zhu, S. Wang, W. Zhang, J. Zhou, Y. Xu, Y. Huang and Y. Wang, *Biomaterials*, 2011, 32, 9707-9718.
3. C. Wu, Y. Luo, G. Cuniberti, Y. Xiao and M. Gelinsky, *Acta biomaterialia*, 2011, 7, 2644-2650.
4. A. Löber, A. Verch, B. Schlemmer, S. Höfer, B. Frerich and M. R. Buchmeiser, *Angewandte Chemie International Edition*, 2008, 47, 9138-9141.
5. B. Basu, *Materials Technology: Advanced Biomaterials*, 2014, 29, B2-B3.
6. M. Zhu, L. Zhang, Q. He, J. Zhao, G. Limin and J. Shi, *Journal of Materials Chemistry*, 2011, 21, 1064-1072.
7. M. Vallet□Regí and E. Ruiz□Hernández, *Advanced Materials*, 2011, 23, 5177-5218.
8. X. Yan, C. Yu, X. Zhou, J. Tang and D. Zhao, *Angewandte Chemie International Edition*, 2004, 43, 5980-5984.
9. G. Heimke, *Advanced Materials*, 1991, 3, 320-322.
10. X. Li, X. Wang, H. Chen, P. Jiang, X. Dong and J. Shi, *Chemistry of materials*, 2007, 19, 4322-4326.
11. H.-s. Yun, S.-e. Kim and Y.-t. Hyeon, *Chemical Communications*, 2007, 2139-2141.
12. Y. Zhu, Y. Zhang, C. Wu, Y. Fang, J. Yang and S. Wang, *Microporous and Mesoporous Materials*, 2011, 143, 311-319.
13. C. Wu, Y. Zhang, Y. Zhu, T. Friis and Y. Xiao, *Biomaterials*, 2010, 31, 3429-3438.
14. J. R. Jones, L. M. Ehrenfried and L. L. Hench, *Biomaterials*, 2006, 27, 964-973.
15. S. Ghosh, S. T. Parker, X. Wang, D. L. Kaplan and J. A. Lewis, *Advanced Functional Materials*, 2008, 18, 1883-1889.
16. Q. Fu, M. N. Rahaman, B. Sonny Bal, R. F. Brown and D. E. Day, *Acta Biomaterialia*, 2008, 4, 1854-1864.
17. A. Goyanes, C. Souto and R. Martínez-Pacheco, *Pharmaceutical development and technology*, 2013, 18, 137-145.
18. S. Mallick, S. Pattnaik, K. Swain, P. K. De, A. Saha, G. Ghoshal and A. Mondal, *European Journal of Pharmaceutics and Biopharmaceutics*, 2008, 68, 346-351.
19. T. Ballet, L. Boulange, Y. Brechet, F. Bruckert and M. Weidenhaupt, *Bulletin of the Polish Academy of Sciences: Technical Sciences*, 2010, 58, 303-313.
20. D. Wanna, C. Alam, D. M. Toivola and P. Alam, *Advances in Natural Sciences: Nanoscience and Nanotechnology*, 2013, 4, 045002.
21. J. Margolis, *Journal of clinical pathology*, 1958, 11, 406.
22. D. S. Véliz, C. Alam, D. M. Toivola, M. Toivakka and P. Alam, *Colloids and Surfaces B: Biointerfaces*, 2014.
23. C. Nwoye, K. Okeke, C. Nwakwuo, G. Obasi and S. Ofoegbu, *Life Science Journal*, 2010, 7.
24. L. Xia, D. Zeng, X. Sun, Y. Xu, L. Xu, D. Ye, X. Zhang, X. Jiang and Z. Zhang, *Microporous and Mesoporous Materials*, 2013, 173, 155-165.
25. C. Xue, J. Wang, B. Tu and D. Zhao, *Chemistry of Materials*, 2009, 22, 494-503.
26. K. Kaewtatip, V. Tanrattanakul and W. Phetrat, *Applied Clay Science*, 2013, 80, 413-416.
27. R. Sukumar and A. Menon, *Journal of applied polymer science*, 2008, 107, 3476-3483.
28. B. Fabbri, S. Gualtieri and C. Leonardi, *Applied Clay Science*, 2013, 73, 2-10.
29. H.-s. Yun, S.-e. Kim, Y.-t. Hyun, S.-j. Heo and J.-w. Shin, *Chemistry of Materials*, 2007, 19, 6363-6366.
30. M. M. Pereira, A. E. Clark and L. L. Hench, *Journal of the American Ceramic Society*, 1995, 78, 2463-2468.
31. A. Hoppe, N. S. Güldal and A. R. Boccaccini, *Biomaterials*, 2011, 32, 2757-2774.
32. S. P. Low, K. A. Williams, L. T. Canham and N. H. Voelcker, *Biomaterials*, 2006, 27, 4538-4546.
33. W. Zhang, G. Wang, Y. Liu, X. Zhao, D. Zou, C. Zhu, Y. Jin, Q. Huang, J. Sun and X. Liu, *Biomaterials*, 2013, 34, 3184-3195.
34. J. Wei, J. Jia, F. Wu, S. Wei, H. Zhou, H. Zhang, J.-W. Shin and C. Liu, *Biomaterials*, 2010, 31, 1260-1269.
35. H. Xia, F. Xia, Y. Tang, W. Guo, X. Hou, L. Chen, Y. Hou, G. Zhang and L. Jiang, *Soft Matter*, 2011, 7, 1638-1640.
36. H. Zreiqat, S. M. Valenzuela, B. B. Nissan, R. Roest, C. Knabe, R. J. Radlanski, H. Renz and P. J. Evans, *Biomaterials*, 2005, 26, 7579-7586.
37. L. L. Hench, *Journal of the European Ceramic Society*, 2009, 29, 1257-1265.
38. P. Han, C. Wu and Y. Xiao, *Biomaterials Science*, 2013, 1, 379-392.
39. S. Maeno, Y. Niki, H. Matsumoto, H. Morioka, T. Yatabe, A. Funayama, Y. Toyama, T. Taguchi and J. Tanaka, *Biomaterials*, 2005, 26, 4847-4855.
40. S. Maeno, Y. Niki, H. Matsumoto, H. Morioka, T. Yatabe, A. Funayama, Y. Toyama, T. Taguchi and J. Tanaka, *Biomaterials*, 2005, 26, 4847-4855.
41. J. Guan, M. S. Sacks, E. J. Beckman and W. R. Wagner, *Biomaterials*, 2004, 25, 85-96.
42. G. Kumar, C. K. Tison, K. Chatterjee, P. S. Pine, J. H. McDaniel, M. L. Salit, M. F. Young and C. G. Simon Jr, *Biomaterials*, 2011, 32, 9188-9196.

Graphical Abstract:

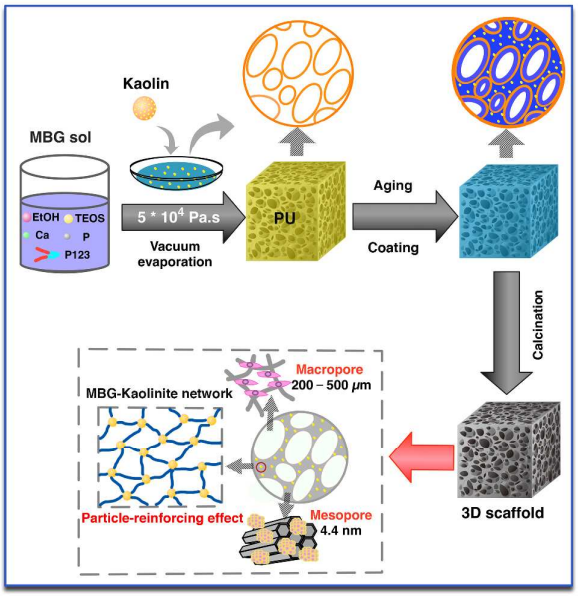

In this study, mechanically stable MBG-XK scaffolds with hierarchical porous structure and excellent biologic performance were prepared via a facile multi-template method with Kaolin as reinforcing agent. The developed MBG-XK scaffolds with 85% porosity exhibited robust mechanical strength with highly interconnected macroporous networks (200 μm-500 μm) and well-defined mesoporous structure (4.4 nm). Moreover, with addition of Kaolin, the MBG-10K scaffold exhibited a more stable and desirable pH environment while maintained the apatite formation ability on the surface. With rBMSCs as model, in vitro cell culture experiments indicated that compared with MBG, the prepared MBG-10K scaffold possessed comparable cell proliferation, penetration capacity and enhanced cell attachment as well as osteogenic differentiation.